IOPscience iopscience.iop.org

Home Search Collections Journals About Contact us My IOPscience

Localized oblique-angle deposition: Ag nanorods on microstructured surfaces and their SERS characteristics

This article has been downloaded from IOPscience. Please scroll down to see the full text article.

2011 Nanotechnology 22 505302

(http://iopscience.iop.org/0957-4484/22/50/505302)

View the table of contents for this issue, or go to the journal homepage for more

Download details:
IP Address: 202.40.139.167
The article was downloaded on 19/09/2013 at 04:26

Please note that terms and conditions apply.

Nanotechnology **22** (2011) 505302 (7pp) doi:10.1088/0957-4484/22/50/505302

# Localized oblique-angle deposition: Ag nanorods on microstructured surfaces and their SERS characteristics

**J Fu, Z Cao and L Yobas**

Department of Electronic and Computer Engineering, Hong Kong University of Science and Technology, Clear Water Bay, Hong Kong

E-mail: eelyobas@ust.hk

Received 27 July 2011, in final form 15 October 2011
Published 23 November 2011
Online at stacks.iop.org/Nano/22/505302

**Abstract**
In this paper, we demonstrate a simple and convenient method of depositing Ag nanorods on a substrate inside a standard evaporation chamber with the substrate resting on a leveled stage. Microstructuring the substrate prior to the deposition imparts a large incidence angle (>70°) between the collimated vapor atoms and the local surface normal, which is essential to induce the shadowing effect. Thereby, a localized oblique-angle deposition (LOAD) is realized, forming nanorods selectively on the steep sidewalls of surface microcavities patterned via standard photolithography and silicon dry etching. We also demonstrate that these nanorods can boost SERS activity of the underlying substrate and thus perform comparable to those fabricated via advanced patterning techniques or conventional OAD whereby the entire substrate has to be tilted with respect to the incident vapor atoms. Our results suggest the viability of decorating microchannel sidewalls with SERS-active nanorods for integrated sample processing and SERS detection.

(Some figures may appear in colour only in the online journal)

## 1. Introduction

Surface-enhanced Raman scattering (SERS) has generated considerable interest due to its capability of detecting vibration spectra of molecules down to single-molecule sensitivity [1, 2]. SERS, being a label-free spectroscopic technique, has gained popularity among chemical and biological analyses including detection of proteins [3], DNA [4], bacteria [5] and cells [6]. The technique is typically observed for molecules near a metal surface, especially noble metals (e.g. Ag, Au) and identified with a large boost in their weak Raman scattering signal. Typical enhancement factors are of the order of $10^6$–$10^7$ but can reportedly reach to $10^{14}$ [1]. Such dramatic enhancement brings Raman spectroscopy on par with fluorescence detection in terms of scattering cross sections of molecules.

SERS, although its underlying mechanism is unclear, is mainly attributed to the signal amplification through electromagnetic (EM) and chemical means [7]. The former is associated with a phenomenon known as localized surface plasmon resonance (LSPR) and considered as the major contributor [8]. When a radiation excites the plasmonic structures, their conduction electrons collectively oscillate and induce an enhanced field near the surface. The chemical amplification occurs, to a lesser extent, when a charge transfer from a metal surface to an adsorbate initiates electronic resonance. Nanostructures well known for their LSPR properties also manifest a reasonable SERS activity. These include aggregates of Ag or Au nanoparticles, nanoshells in suspension or immobilized on substrates [9–12], thin film Ag or Au island deposits [13], Ag or Au thin film metals that are electrochemically roughened [14] or directly deposited on porous or template-structured substrates such as porous silicon [15], nanowires [16], nanotips [17], nanograss [18] and nanorods [19]. For the articulated nanostructures, the bottom-up fabrication techniques may involve chemical reduction or high-power laser ablation of nanoparticles whereas the top-down techniques are chosen from various forms of lithography (e.g. deep UV, electron beam, nanosphere and nanoimprint).

Recently, Ag nanorod arrays fabricated by oblique-angle deposition (OAD) have been found to exhibit a fairly strong SERS response [20]. As schematically described in figure 1(a), OAD is a physical vapor deposition technique in which the

 © 2011 IOP Publishing Ltd Printed in the UK & the USA

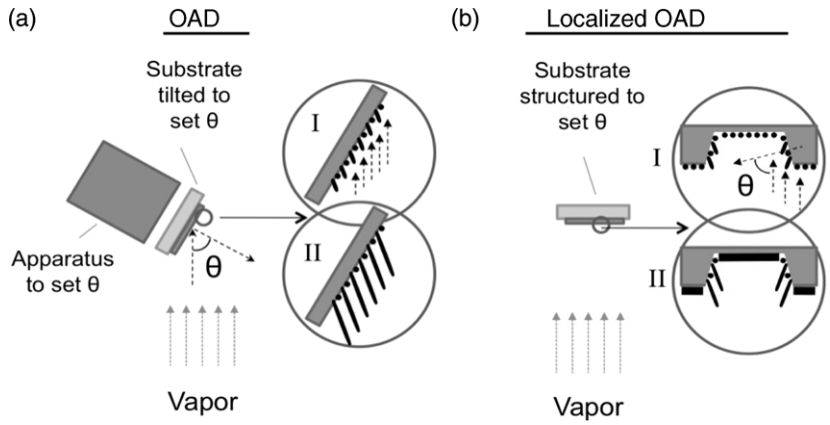


**Figure 1.** Schematics comparing nanorod formation through the process of (a) oblique-angle deposition (OAD) and (b) localized OAD (LOAD). Insets: (I) earlier in the process, nucleation points tend to form islands of unequal heights on the surface; (II) later in the process, islands grown taller limit the growth of those adjacent by intercepting their supply of the collimated vapor atoms. The angle $\theta$ preferably exceeds 70° measured between the incident collimated beam of vapor flux and local surface normal.

incident metal vapor atoms are deposited on a substrate at a large incidence angle ($\theta > 70°$) with respect to the surface normal of the substrate. As the incident vapor atoms nucleate on the substrate, they create sites of preferential growth that further shadow the regions behind them. Due to limited diffusion of adatoms, the so-called shadowing effect gives way to voids and consequent formation of a thin film columnar structure with nanorods [21]. The OAD process, as it does not ask for a high-resolution lithography, is an attractive method to produce functional nanostructures. Nevertheless, the technique requires tilting the entire substrate with respect to the incident vapor atoms so as to set the desired incidence angle.

In contrast, the OAD process is modified here such that it can be implemented in a standard tool with the substrate held on a leveled stage. The large incidence angle ($\theta > 70°$) required for creating the shadowing effect and the subsequent formation of columnar nanostructures is imparted to the surface by microstructuring the substrate prior to the deposition. Consequently, a localized oblique-angle deposition (LOAD) is observed with Ag nanorods appearing selectively on the steep sidewalls of the etched surface microcavities on silicon (figure 1(b)). Morphology of the Ag nanorods and their SERS spectroscopy are presented through scanning electron microscopy images and Raman peaks obtained with Rhodamine B (RhB) molecules as the adsorbate.

## 2. The experiment

The substrates were prepared by patterning a 1 $\mu$m thick photoresist layer as an etch mask on p-type silicon wafers (100 mm diameter and ⟨100⟩ oriented) via UV-lithography. The wafers were then structured with regular arrays of microcavities through isotropic dry etching. Upon stripping the photoresist, the wafers were further etched via deep reactive ion etching (DRIE) to remove about 1.6 $\mu$m thick bulk silicon from the entire surface. This extra etch was applied to eliminate the overhanging silicon regions masking the sidewalls. The wafers were then diced into 1 cm × 1 cm chips. The individual chips were placed on a leveled stage in a standard e-beam evaporator (Peva-600EI) and deposited with Ag (99.999%, Kurt J Lesker Co.) under vacuum ($<10^{-7}$ Torr). The deposition rates and thicknesses were confirmed with a quartz crystal microbalance (QCM). Some of the chips received *a priori* deposition of a thin film Ag (base layer) through sputtering (ARC-12M). The sputtered atoms, as they are scattered in all directions, did not lead to significant shadowing. The chips were incubated with RhB dissolved in methanol for the indicated period of time, subsequently dried in air and, unless otherwise stated, immediately probed for SERS activity under a Raman microscope (RM3000, Renishaw) equipped with a near-infrared diode laser source (785 nm and 300 mW). The laser beam was focused on an elliptic spot (∼5 $\mu$m × 20 $\mu$m) through a 50× objective, delivering 2 mW power (Lasercheck, Coherent Inc.). The Raman spectra were obtained after one accumulation (total time 10 s).

## 3. Results and discussion

### *3.1. Morphology*

In figure 2, scanning electron microscopy (SEM) images of separate chips reveal the three distinct microcavity patterns structured on silicon prior to Ag deposition. The cross-sectional profile of a representative microcavity from each chip is also shown. The three patterns, namely P1, P2 and P3, feature identical microcavities at a pitch of 5 $\mu$m, 10 $\mu$m and 20 $\mu$m, respectively, all isotropically etched through 2 $\mu$m diameter openings in a photoresist layer. The isotropic etching profile, however, led to larger microcavities 4.5 ± 0.5 $\mu$m in diameter (∼3 $\mu$m deep) and thus reduced the edge-to-edge separation to 0.35 ± 0.5 $\mu$m, 5 ± 0.5 $\mu$m and 15 ± 0.5 $\mu$m, respectively. The steep profile of the microcavity sidewalls promoted the shadowing effect during collimated Ag evaporation although the chips were held on a leveled stage inside a standard electron-beam evaporation chamber. As a natural outcome of the sidewall slope, a maximum incidence angle of 83.6° ± 1.4° was imposed between the local surface normal and the collimated vapor atoms and thereby leading to the localized oblique-angle deposition (LOAD).

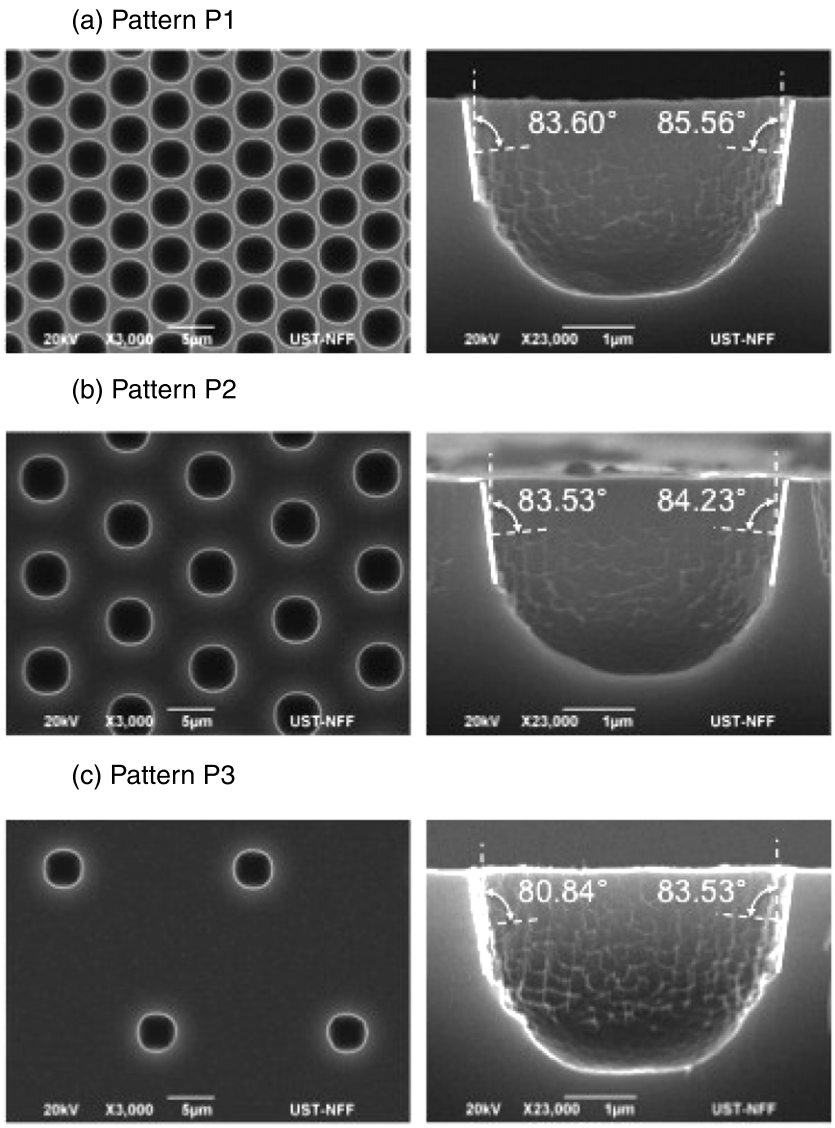


**Figure 2.** Scanning electron microscopy (SEM) images of representative three silicon chips structured with distinct patterns of microcavities shown prior to the Ag deposition step for nanorod formation. The layout patterns (a) P1 (b) P2 and (c) P3 (the left column; all scales: 5 $\mu$m) are distinct in their pitch densities, 5 $\mu$m, 10 $\mu$m and 20 $\mu$m, respectively, yet more or less identical in microcavity cross-sectional profiles (the right column; all scales: 1 $\mu$m).

The LOAD process has been applied to the microcavities by evaporating Ag directly either on a base layer of thin-film-sputtered Ag (process A) or on bare silicon (process B). The investigation also included those with the Ag base layer and yet spared from the subsequent Ag evaporation (process C). Representative microcavities randomly chosen from three separate chips having the same pattern (P1) are depicted by SEM images from isometric and cross-sectional views in figure 3. Given their distinct deposition processes (A, B or C), the microcavities are shown to have inherited a unique morphology. Those having undergone the LOAD (1 $\mu$m thick Ag evaporation) step in process A or B exhibit nanorods on their steep sidewalls. In contrast, those subjected to sputtering through process C (500 nm thick Ag) have only few granular nanostructures confined to their base regions. Process A is distinct from B in that it involves a base layer of 500 nm thick sputtered Ag which is probably why the nanorods exhibit slightly different morphology: 573$\pm$84 nm versus 572$\pm$71 nm in length and 64 $\pm$ 12 nm versus 97 $\pm$ 37 nm in width, respectively.

### *3.2. SERS measurements*

The chips have been probed for SERS activity after having an overnight incubation in RhB solution ($10^{-4}$ M) for spectroscopic analysis. Typical SERS spectra are given in figure 4. In figure 4(a), the inset shows a plot from a blank silicon chip underwent deposition process A. The plot indicates no discernible Raman peak either before or after the incubation with RhB. Figure 4(a) further reveals the spectrum obtained with microcavities of pattern P1 subjected to process A. As shown, five clear peaks emerge upon incubation with RhB, corresponding to the known Raman shifts of the RhB molecule at 1208 (aromatic C–H bending), 1282 (C–C bridge-bands

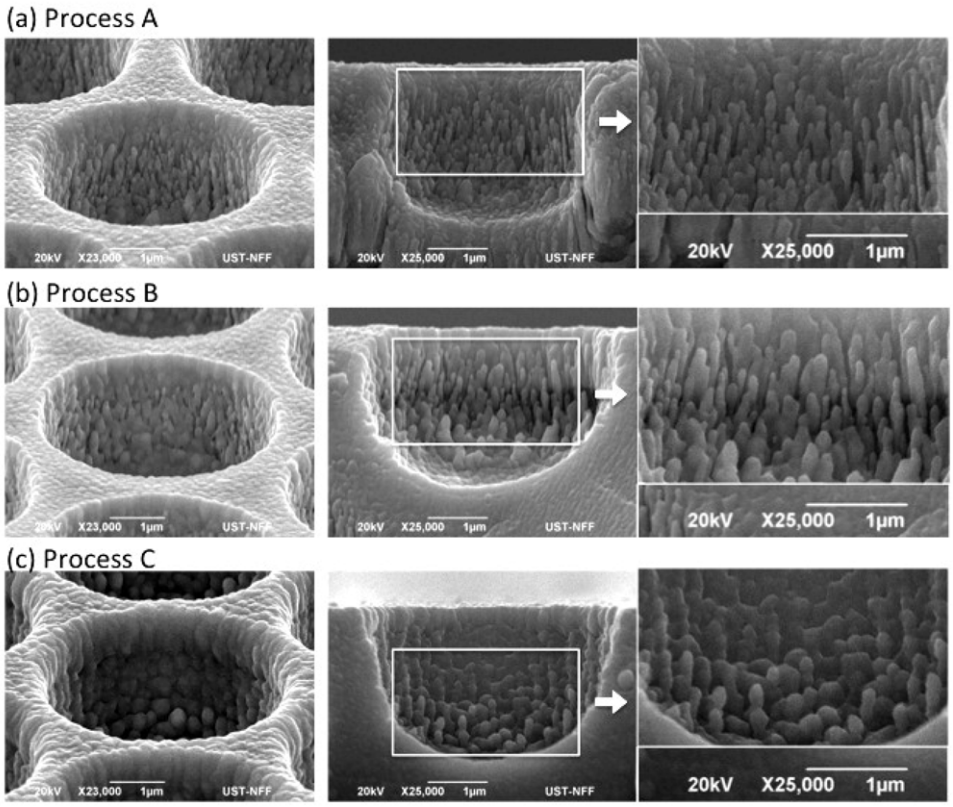


**Figure 3.** SEM images of microcavities (isometric and cross-sectional views including a magnified section demarcated by a white rectangle to show nanostructures) representing structured silicon chips, all according to pattern P1 and yet underwent a distinct process of Ag deposition: (a) process A: 1 $\mu$m thick Ag evaporation on a base layer of 500 nm thick Ag film sputtered on silicon; (b) process B: 1 $\mu$m thick Ag evaporation on silicon; and (c) process C: 500 nm thick Ag film sputtered on silicon. Scales: 1 $\mu$m.

stretching), 1362 (aromatic C–C stretching), 1511 (aromatic C–C stretching) and 1651 (aromatic C–C stretching), all in $cm^{-1}$. These Raman lines more or less agree with the previous reports of the RhB spectrum [4, 22–26]. Figure 4(b) evaluates the spectra obtained with the microcavities of the three distinct patterns (P1, P2 and P3) which received the same deposition (process A). P1 stands out with a much greater SERS enhancement. Among the three patterns, the peak intensities correlate well with their respective pitch densities: the denser the microcavities, the denser the nanorods (and the hot spots) within the incident laser beam and the greater the Raman enhancement.

To assess how much of this enhancement can be attributed to the microcavities (besides the nanorods), figure 4(c) compares the Raman peaks obtained with the representative microcavities which were processed differently (A, B and C) and yet had the same pattern (P1). As seen, the enhancement cannot be attributed to the microcavities; despite all having the same pattern (P1), those having denser and finer nanorod morphology (process A) offer a superior enhancement than those with coarser nanostructures (process B). This suggests that the base layer of sputtered Ag film, apart from leading to denser and finer nanorods, could also play a crucial role in the observed Raman enhancement. Indeed, stronger SERS intensities have also been noticed for the nanorods prepared via OAD on a base layer Ag (100 nm thin) and attributed to the increase in the substrate reflectivity with the base layer [27]. A thicker Ag film (500 nm), since it offers a higher reflectivity, has been utilized here. A more than threefold increase in the intensity observed here with reference to the Raman peak at 1511 $cm^{-1}$ (figure 4(d)) corroborates well with the earlier report [27]. Nevertheless, the increase in the intensity with the remaining patterns (P2 and P3) (figure 4(d)) is not that appreciable, possibly due to the low-density arrangement of the microcavities and the nanorods. The base layer alone without the nanorods (process C) does not lead to much enhancement: Raman peaks are barely noticeable in figure 4(c) and likely to emanate from the granular nanostructures found closer to the bottom of the microcavities (figure 3(c)).

The Raman enhancement by the Ag nanorods prepared via OAD has reportedly shown strong dependence on the deposition angle and the length of Ag nanorods [28]. For instance, a 2° increment in the deposition angle between 80° and 84° produces almost an order-of-magnitude increase in the surface enhancement factor (EF) for the nanorods of the same length (≈160 nm). However, for the nanorods 500–750 nm long, this angle dependence gets considerably less. Since the deposition angle varies with the sidewall slope of the microcavities (83.6° ± 1.4°), a slight etching non-uniformity and the subsequent variation across the microcavity profiles could lead to large fluctuations in the EF value. Thus, the nanorods were deposited here at a length of ≈570 nm for a more uniform substrate-wide enhancement. For the two deposition angles 82° and 84°, the reported optimum lengths

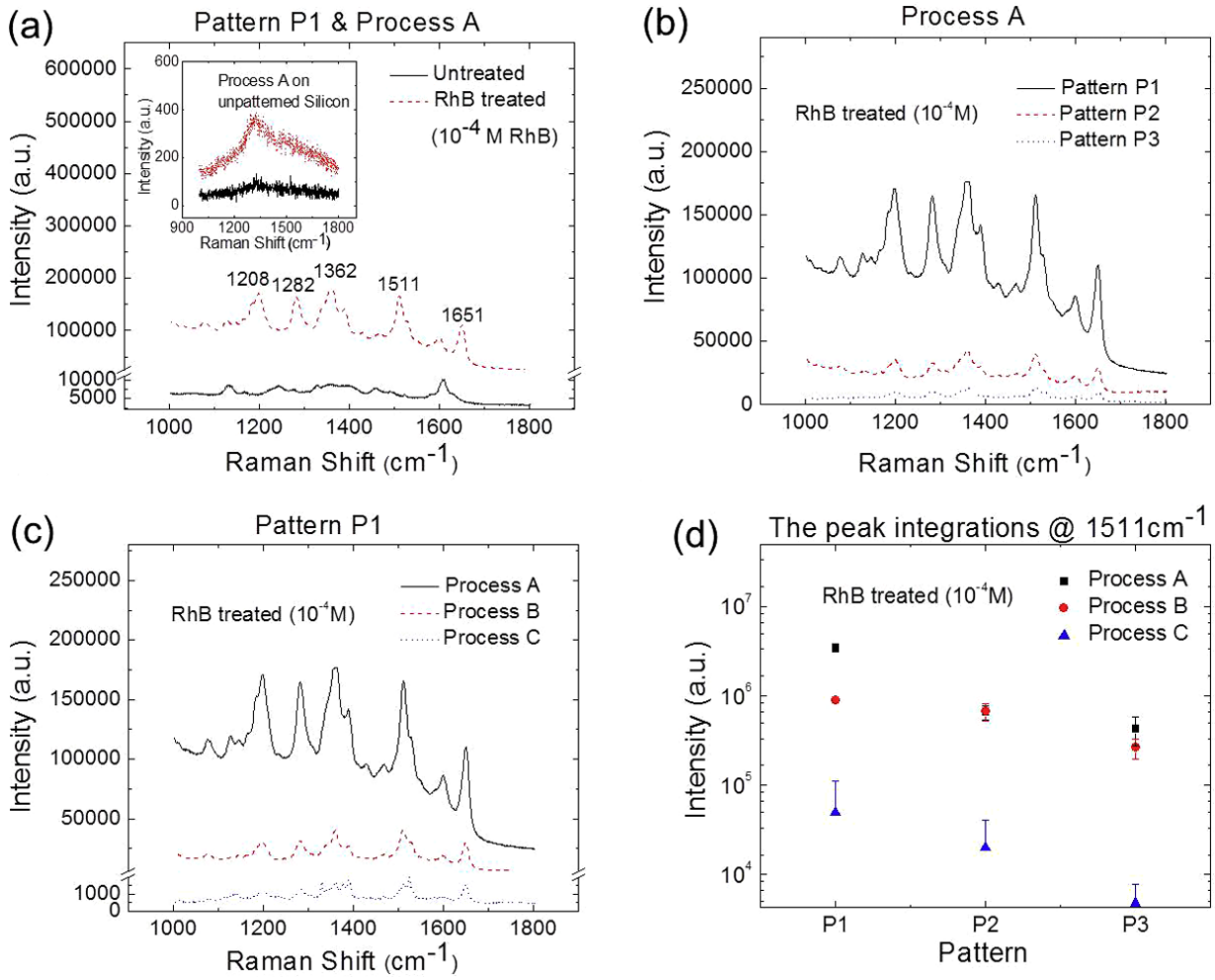


**Figure 4.** SERS spectra of $10^{-4}$ M RhB dye molecules adsorbed on silicon chips fabricated according to (a) process A on pattern P1 shown before and after RhB treatment (inset: process A on a substrate without a pattern); (b) process A on patterns P1, P2 and P3; (c) processes A, B and C on pattern P1 and (d) log-plot comparing integrated peak intensities at 1511 $cm^{-1}$.

are, respectively, 660 nm to 1100 nm and their EF values are at least an order of magnitude apart in favor of the longer nanorods [28]. Since these angles fall within the range of our etching non-uniformity, the nanorods twice as long (≈1140 nm) were also prepared by increasing the deposition duration of processes A and B (2 $\mu$m thick Ag film on QCM). These deposition processes are appropriately categorized as D and E. The substrates, with their identical patterns (P1) and yet distinct deposition processes (A, B, D and E) were incubated in RhB solution ($10^{-4}$ M) longer for about 24 h. Moreover, they were subjected to copious wash in deionized water to remove physically adsorbed molecules. Upon this treatment, it was assumed that their surfaces adsorbed a monolayer of RhB molecules. The SERS intensities were evaluated using the Raman peaks at 1282 and 1511 $cm^{-1}$. However, in contrast with the results of the previous study [28], the integrated intensities with the longer nanorods, (processes D versus A or E versus B in figure 5) have been found slightly weaker.

### *3.3. Calculation of SERS enhancement*

The EF values have been determined here based on the common definition: $EF = N_R I_{SERS}/N_{SERS} I_R$, where $N_R$ and $N_{SERS}$ are the total counts of RhB molecules that are excited by the laser beam in solution and adsorbed on the substrate, respectively, whereas $I_R$ and $I_{SERS}$ are the corresponding integrated intensities at the indicated Raman shifts. The total counts of RhB molecules contributing to the Raman peaks can be estimated as $1.0 \times 10^6$ ($N_{SERS}$) for the substrates (pattern P1) and $6.02 \times 10^{10}$ ($N_R$) for the bulk solution (0.1 M) under the following assumptions: (1) the size of a single molecule is 1.6 nm in diameter [29]; (2) the molecules are chemically adsorbed on the nanorods forming a monolayer coverage of 1 $\mu m^2$/microcavity (four microcavities of pattern P1 fit in a laser spot); and (3) the microscope optically samples a ∼1 pl focal volume of the bulk solution. The representative Raman spectra obtained with the prepared substrates and with the bulk solution are shown in figure 6. Table 1 lists the EF values calculated accordingly with reference to the peak intensities at 1282 and 1511 $cm^{-1}$. The values are of the order of $10^5$ and comparable to those reported for the Ag nanorods fabricated via OAD (i.e. on unstructured substrates) [20, 28].

The experiments with Ag nanorod arrays on unstructured planar substrates (through OAD) have revealed three interesting SERS characteristics [30]: (1) the incident angle dependence [31], (2) the substrate reflectivity dependence [20, 27]

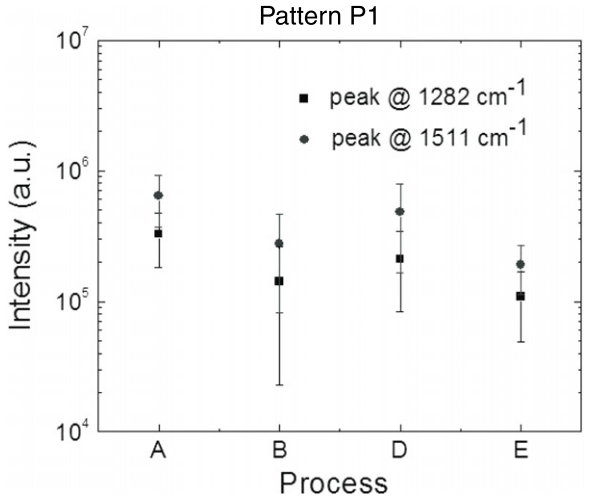


**Figure 5.** A log-plot comparing integrated peak intensities of Raman lines at 1282 and 1511 $cm^{-1}$ for $10^{-4}$ M RhB dye molecules adsorbed on the silicon chips fabricated through processes A, B, D and E, all with pattern P1. Process D: 2 $\mu$m thick Ag film evaporated on a 500 nm thick Ag film sputtered on a structured silicon substrate. Process E: 2 $\mu$m thick Ag film evaporated on a structured silicon substrate.

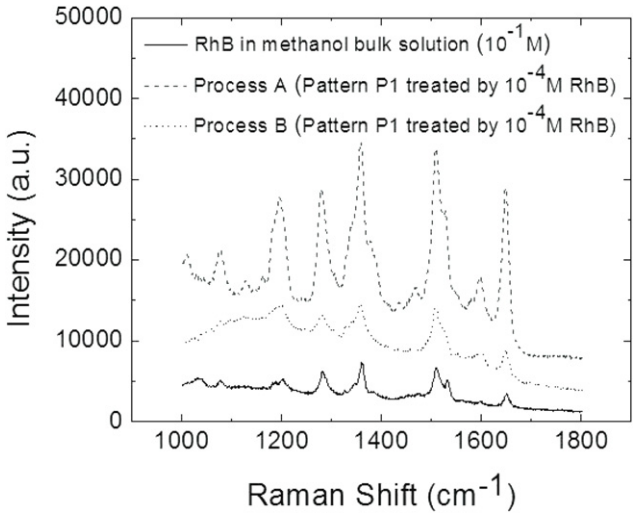


**Figure 6.** Raman spectra of RhB molecules (a) in methanol bulk solution (0.1 M), (b) and (c) chemically adsorbed on silicon chips fabricated through process A and process B, respectively. All the chips were imprinted with pattern P1. They were incubated in RhB solution ($10^{-4}$ M) for a day and subsequently washed in deionized water to remove physically adsorbed molecules.

and (3) the polarization dependence [32]. It has been shown that the SERS intensity reaches a maximum at an incident angle of the excitation laser ∼45° relative to the substrate normal; an eightfold increase in the intensity has been reported as compared to that observed with the excitation laser normal to the substrate. It should be noted that the nanorods in those measurements are tilted ∼73° from the substrate normal as a result of the vapor deposition angle 86°. However, in the method described here, the substrates are held on a leveled stage during deposition as well as SERS measurement. Thus, both the vapor and the excitation incident angles are the same and determined by the sidewall slope of the microcavities (≈84°). The optimum excitation angle is likely to vary with the substrate profile and should be further investigated for the nanorods here. In addition, the nanorods on the steep sidewalls of the microstructures might use enhancement mechanisms different from the nanorods on unstructured substrates. For the latter, the investigators argue that the structure and the layer absorbance, rather than the hot spots, play a dominant role since the hot spots in those nanorods do not directly face the detector [33]. This may not be the case for the nanorods here owing to their distinct configuration.

**Table 1.** The integrated Raman peak intensities and the calculated EF values based on figure 6.

| Target specimen | $I_{R,SERS}$ ($\times 10^5$) | | EF ($\times 10^5$) | |
|---|---|---|---|---|
| | 1282 $cm^{-1}$ | 1511 $cm^{-1}$ | 1282 $cm^{-1}$ | 1511 $cm^{-1}$ |
| Si chip I (process A) | 3.27 | 6.41 | 3.43 | 3.36 |
| Si chip II (process B) | 1.43 | 2.73 | 1.50 | 1.43 |
| RhB bulk solution (0.1 M) | 0.58 | 1.15 | — | — |

## 4. Conclusion

In summary, a simple and convenient method of fabricating functional Ag nanorods is demonstrated. The method, while it is based on OAD, is easily implemented in a readily available standard deposition chamber without the requirement of tilting the substrate. To create the shadowing effect during deposition and to subsequently form the nanorods, the method imparts a large incidence angle between the vapor atoms and the local surface normal by microstructuring the substrate. In return, a localized OAD (LOAD) is realized, forming nanorods selectively on the steep sidewalls of the surface microstructures, which can be simply patterned on the substrate using standard tools and without the need for high-resolution advanced lithography techniques. Furthermore, functionality of the nanorods has been verified by unraveling their SERS activity on the Raman probe molecule RhB. The nanorods on a high-density array of microcavities in silicon have been shown to considerably increase the SERS activity of the underlying substrate with enhancement factors reaching those reported for the nanorods fabricated through the conventional OAD. The method, therefore, offers a simple route to producing SERS-active substrates in standard facility settings. Our future work will involve applying LOAD to decorate microchannel sidewalls with Ag nanorods for an integrated sample processing and SERS detection.

## Acknowledgment

The authors thank Dr B Shi for his help with the Raman microscopy.

## References


[1] Nie S M and Emery S R 1997 *Science* **275** 1102
[2] Kneipp K, Wang Y, Kneipp H, Perelman L T, Iztkan I, Dasari R R and Feld M S 1997 *Phys. Rev. Lett.* **78** 1667
[3] Xu H X, Bjerneld E J, Kall M and Borjesson L 1999 *Phys. Rev. Lett.* **83** 4357
[4] Allain L R and Vo-Dinh T 2002 *Anal. Chim. Acta* **469** 149
[5] Jarvis R M and Goodacre R 2004 *Anal. Chem.* **76** 40
[6] Huang X, El-Sayed H, Qian W and El-Sayed M A 2007 *Nano Lett.* **7** 1591
[7] Moskovits M 1985 *Rev. Mod. Phys.* **57** 783
[8] Dieringer J A, McFarland A D, Shah N C, Stuart D A, Whitney A V, Yonzon C R, Young M A, Zhang X and Van Duyne R P 2006 *Faraday Discuss.* **132** 9
[9] Faulds K, Littleford R E, Graham D, Dent G and Smith E W 2004 *Anal. Chem.* **76** 592
[10] Talley C E, Jackson J B, Oubre C, Grady N K, Hollars C W, Lane S M, Huser T R, Nordlander P and Halas N J 2005 *Nano Lett.* **5** 1569
[11] Jackson J B and Halas N J 2004 *Proc. Natl Acad. Sci. USA* **101** 17930
[12] Wang H, Levin C S and Halas N J 2005 *J. Am. Chem. Soc.* **127** 14992
[13] Van Duyne R P, Hulteen J C and Treichel D A 1993 *J. Chem. Phys.* **99** 2101
[14] Liu Y-C, Yu C-C and Sheu S-F 2006 *J. Mater. Chem.* **16** 3546
[15] Chan S, Kwon S, Koo T-W, Lee L P and Berlin A A 2003 *Adv. Mater.* **15** 1595
[16] Fang C, Agarwal A, Ji H, Karen W Y and Yobas L 2009 *Nanotechnology* **20** 405604
[17] Guieu V, Lagugné-Labarthet F, Servant L, Talaga D and Sojic N 2008 *Small* **4** 96
[18] Tang J, Ou F S, Kuo H P, Hu M, Stickle W F, Li Z and Williams R S 2009 *Appl. Phys.* A **96** 793
[19] Nikoobakht B and El-Sayed M A 2003 *J. Phys. Chem.* A **107** 3372
[20] Chaney S B, Shanmukh S, Dluhy R A and Zhao Y-P 2005 *Appl. Phys. Lett.* **87** 031908
[21] Abelmann L and Lodder C 1997 *Thin Solid Films* **305** 1
[22] Zhang J, Li X, Sun X and Li Y 2005 *J. Phys. Chem.* B **109** 12544
[23] Fang C, Agarwal A, Buddharaju K D, Khalid N M, Salim S M, Widjaja E, Garland M V, Balasubramanian N and Kwong D-L 2008 *Biosens. Bioelectron.* **24** 216
[24] Vo-Dinh T, Yan F and Wabuyele M B 2005 *J. Raman Spectrosc.* **36** 640
[25] Wang G, Lim C, Chen L, Chon H, Choo J, Hong J and deMello A 2009 *J. Anal. Bioanal. Chem.* **394** 1827
[26] Geiman I, Leona M and Lombardi J R 2009 *J. Forensic Sci.* **54** 947
[27] Zhou Q, Liu Y, He Y, Zhang Z and Zhao Y 2010 *Appl. Phys. Lett.* **97** 121902
[28] Liu Y-J, Chu H Y and Zhao Y-P 2010 *J. Phys. Chem.* C **114** 8176
[29] Tsunomori F and Ushiki H 1999 *Phys. Lett.* A **258** 171
[30] Liu Y-J and Zhao Y-P 2008 *Phys. Rev.* B **78** 075436
[31] Liu Y-J, Fan J-G, Zhao Y-P, Shanmukh S and Dluhy R A 2006 *Appl. Phys. Lett.* **89** 173134
[32] Zhao Y-P, Chaney S B, Shanmukh S and Dluhy R A 2006 *J. Phys. Chem.* B **110** 3153
[33] Zhang Z-Y, Liu Y-J, Zhao Q and Zhao Y-P 2009 *Appl. Phys. Lett.* **94** 143107